# Finding Leaves in the Forest: The Dual-Wavelength Echidna Lidar

Ewan S. Douglas, Jason Martel, Zhan Li, Glenn Howe, Kuravi Hewawasam, Robert A. Marshall, Crystal L. Schaaf, Timothy A. Cook, Glenn J. Newnham, Alan Strahler, and Supriya Chakrabarti

***Abstract*—The dual-wavelength Echidna lidar is a portable ground-based full-waveform terrestrial scanning lidar for characterization of fine-scale forest structure and biomass content. While scanning, the instrument records the full time series of returns at a half-nanosecond rate from two coaligned 5-ns pulsed lasers at 1064 and 1548 nm wavelengths. Leaves absorb more strongly at 1548 nm compared to stems, allowing discrimination of forest composition at milliradian scales from the ground to the forest canopy. This work describes the instrument design and data products and demonstrates the power of two wavelength lidar to clearly distinguish leaves from woody material with preliminary field data from the Sierra Nevada National Forest.**

***Index Terms*—Forestry, laser radar, vegetation mapping.**

## I. Introduction

A RECENTLY commissioned terrestrial forest scanning lidar, the dual-wavelength Echidna lidar (DWEL), characterizes forest structure at fine spatial scales while distinguishing between leaves and trunks. Improving the design of the Echidna validation instrument (EVI), conceived and constructed by Australia's Commonwealth Scientific and Industrial Research Organization (CSIRO) [1], DWEL adds dual-wavelength target discrimination and increased portability. Similar to EVI, DWEL uses a slowly rotating azimuth platform and a rapidly rotating altitude scan mirror with continuous half-nanosecond digitization of return waveforms from short laser pulses at 1064 nm to identify targets in nearby 3-D space. DWEL adds a second coaxial laser pulse at 1548 nm, which is more readily absorbed by leaves. The resulting data set can be utilized to determine forest structural parameters, including the mean tree diameter at breast height, stem count density (trees per hectare), basal area, canopy height, leaf area index, foliage profile, and above-ground biomass using the approaches pioneered in the development and application of EVI [2]–[4]. Scans in close proximity from multiple points within a region of forest can be registered to provide 3-D reconstructions of forests that allow virtual measurements of forest structure [5]. DWEL's coaxial and simultaneous two wavelength ranging can provide direct measurement of material volume and leaf area to estimate both green leaves and woody biomass without allometric equations, improving ground validation of airborne lidar measurements of biomass (e.g., [6]) to calibrate large area studies, such as the National Ecological Observation Network [7].

Manuscript received June 11, 2014; revised September 6, 2014; accepted October 1, 2014. This work was supported by the National Science Foundation under Grant DBI-0923389.

E. S. Douglas is with the Department of Astronomy, Boston University, Boston, MA 02215 USA.

J. Martel, G. Howe, K. Hewawasam, T. A. Cook, and S. Chakrabarti are with the University of Massachusetts Lowell, Lowell, MA 01854 USA.

Z. Li and A. Strahler are with the Department of Earth and Environment, Boston University, Boston, MA 02215 USA.

R. A. Marshall is with the Department of Aeronautics and Astronautics, Stanford University, Stanford, CA 94305-4035 USA.

C. L. Schaaf is with the Department of Environmental, Earth, and Ocean Sciences, University of Massachusetts Boston, Boston, MA 02125 USA.

G. J. Newnham is with CSIRO Land and Water, Acton, ACT 2601, Australia.

Color versions of one or more of the figures in this paper are available online at http://ieeexplore.ieee.org.

Digital Object Identifier 10.1109/LGRS.2014.2361812

## II. Science Drivers

### A. Distinguishing Leaves From Trunks

For spatially unresolved targets, such as distant leaves, distinguishing between leaves and woody biomass with a single wavelength lidar has been attempted from the shape of the full-waveform return [3]. If the return fits the output pulse well, the pulse has hit a hard target, such as a trunk, branch, or the ground. If a return is extended in range, it is more likely to be a collection of leaves. This procedure distinguishes leaves separated more widely than the instrument range confusion limit—the minimum separation between distinguishable hard targets—which depends on a variety of factors, particularly the pulsewidth and the hit extraction technique used. Compact leaf clumps, however, produce "hard hits" that are indistinguishable from trunk and branch hits with a single wavelength.

Additionally, as spatial resolution becomes coarser with increasing range, pulses hitting clusters of branches and the edges of closely spaced trunks are confused with pulses scattered by leaves, which can erroneously increase the inferred leaf signal. Adding a second wavelength to lidar scanning permits target differentiation, independent of target morphology and spatial configuration. A strong spectral contrast exists between leaves and other materials in the shortwave infrared, due to a broad absorption feature arising from stretch O-H and C-H transitions in leaf starch, sugar, lignin, and water and centered at 1450 nm [8]. The depth of this absorption feature in leaves is dominated by the water content [9], and for typical leaf water contents, this absorption acts to lower leaf reflectance at 1548 nm, compared to tree stems. This contrast can be seen in standard spectra of multiple tree species [10]. Comparison of this feature with a reference (1064 nm for DWEL) wavelength allows discrimination between targets.

### B. Range Resolution

Characterizing biomass accurately requires sufficient range resolution to resolve submeter-scale forest structure and to accurately "stitch" together multiple scans into 3-D spaces. Rather than returning intensity and range for discrete hits which exceed a threshold, DWEL records the full return waveform intensity as a function of time at a high cadence. A complete time series to the instrument range limit enables waveform fitting and deconvolution to more accurately determine background noise levels, as well as range and target properties for multiple partial returns in a single waveform.

### C. FOV

DWEL requires a field-of-view (FOV) which balances accurate retrieval with short scanning times. DWEL's design thus calls for outgoing beam divergence to be adjustable between 1 and 5 mrad, and the zenith and azimuth scan motor speeds to be individually set, providing complete angular sampling over a range of beam divergences. This range overlaps with the high-resolution scans of the EVI (which employs a variable divergence of 2–15 mrad).

### D. Portability

Forested environments where the DWEL is expected to be deployed are often remote and have rugged terrain, and typically, vehicular access is difficult. The EVI instrument incorporated a desktop computer and was dependent on a portable internal combustion generator, which limited EVI deployments to environments readily accessible by road. Access is critical to characterization of forest variations; thus, DWEL was designed with the constraint of allowing two researchers to readily carry the instrument through difficult terrain on foot and operate for extended periods of time using batteries.

## III. DWEL Instrument

This section describes the final design of the deployed DWEL instrument.

### A. Design Drivers

*1) Laser Selection:* Laser selection was driven by availability, portability, and safety. The lasers were specified to have a nominal output energy of 0.6 $\mu$J, providing a functional range of $> 70$ m, sufficient to characterize old growth canopies, while minimizing power consumption.

*2) Positional Accuracy:* For determination of target direction with submilliradian precision, a minimum of 14 b of angular resolution was required.

*3) Portability:* The volume and mass were constrained by the carrying capacity of two researchers on foot, one carrying the instrument and the other support equipment (e.g., laptop, batteries, and tripod). This requirement was interpreted as an instrument mass limit of 25 kg including sufficient battery storage for 2 h of operation.

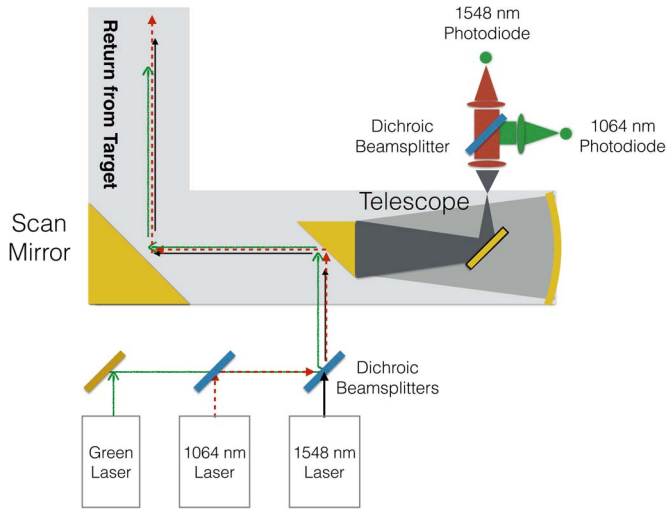


Fig. 1. Instrument schematic. Thin lines represent the outgoing coaxial beams. Gray lines represent the FOV of the instrument and the path of the observed returns. The continuous wave green laser serves as a marker and is not recorded.

TABLE I
LASER PARAMETERS. A SINGLE ASTERISK INDICATES A MANUFACTURER SPECIFICATION, AND TWO ASTERISKS INDICATE A PARAMETER MEASURED DURING DWEL INTEGRATION

| Parameter | 1064 nm | 1548 nm |
|---|---|---|
| Trigger rate** [kHz] | 19.7718± 0.0007 | |
| Pulse energy (typical)* [ $\mu$J ] | 0.6 | |
| Output Pulse Length* [ns] | 5.0 ± 0.1 | |
| Beam Diameter ($1/e^2$) [mm] | 7 * | 7 ** |
| Typical Beam Divergence* [milliradian] | 2.5 | |
| Filter Central Wavelength * [nm] | 1064 ± 2 | 1550 ± 8 |
| Solar filter FWHM* [nm] | 10 ± 2 | 40 ± 8 |

### B. Implementation

*1) Output Optics Layout:* The transmitter and receiver optical layout is shown in Fig. 1. A high-efficiency dichroic beamsplitter, Thorlabs DMLP1180, permits dual-wavelength operation and alignment of the beams coaxially to less than 1 mrad. All reflective surfaces are protected gold. The DWEL lasers were built by Manlight, pulsing wavelengths of 1064 and 1548 nm, with repetition frequencies of 20 kHz, random polarization, and pulse lengths of 5 ns. The lasers are synchronized by externally triggering on a single Linear Technology LTC6990 voltage-controlled oscillator. Table I summarizes the key laser parameters. Typically, instrument resolution values are 1, 2, and 4 mrad. Interchangeable divergence optics, set to 1.25, 2.5, and 5 mrad, expand the outgoing beam at these scan settings, providing continuous coverage of the angular scan sphere. A 5-mW class 3R green laser is included in the optical train as a visible alignment guide.

*2) Beam Profile:* Previous authors (e.g., [1] and [11]) have suggested that the outgoing spatial laser beam profile of the Echidna and DWEL instruments is flat or "top hat" shaped, permitting a constant relation between the return intensity and the fractional area of the beam intercepted by the target. EVI employed an apodizing output filter, intended to transform a

Gaussian beam profile into a 29-mm top hat [12]. Likewise, the original DWEL design called for a high-efficiency optical top hat beam shaper; however, such a profile can necessarily only occur at one distance from the shaping optic. Top hat beam forming is analogous to a plane wave incident on a circular aperture, which results in a geometry-dependent interference pattern. The Fresnel number ($F = a^2/\lambda d$, where, in this case, $\lambda$ is the wavelength, $a$ is the beam radius, and $d$ is the range) dictates the diffraction regime and also can be used as a metric of the top hat beam integrity. The beam will stay nearly top hat when $F \gg 1$, and as the range increases, the pattern will vary according to Fresnel diffraction, whereas in the far field, as $F \ll 1$, Fraunhofer diffraction dominates, and the profile will approach an Airy pattern. At 1548 nm, a 6-mm diameter top hat beam loses integrity within centimeters, and $F$ is equal to 1 at just 6 m. Thus, over a short distance, a top hat beam maintains its intensity distribution but quickly degenerates into a complicated diffraction pattern (for illustrations and a more complete discussion of diffraction due to a circular aperture, see [13]). Consequently, the deployed DWEL design uses a conventional Gaussian beam profile, which propagates smoothly with range and avoids a rapidly varying intensity distribution as a function of range.

*3) Telescope:* The 10-cm rotating scan mirror acts as the first receiving surface, reflecting the return beam into the receiver telescope. The telescope is an f/4.35 Nasmyth–Newtonian optical layout, composed of parabolic primary and flat secondary and tertiary mirrors. The telescope output is recollimated, and the 1064 and 1548 nm beams are split via a dichroic beamsplitter to separate detectors. In front of each detector assembly is a reimaging lens and a narrow-band laser line filter to minimize crosstalk and out-of-band contamination.

*4) Photodiodes:* In order to accommodate the relatively wide FOV necessary to completely sample coarse scans—those with a beam divergence of 5 mrad—a detector with a large surface area was employed. Both channels use fixed-gain Thorlabs PDA10CF amplified InGaAs photodiodes with a 0.2-mm$^2$ active area. The gain bandwidth product and the large surface area limit the diode bandwidth to the manufacturer-reported small-signal bandwidth of DC-150 MHz. This has the effect of smoothing the return pulse recorded from a hard surface, which widens the effective range confusion limit.

*5) Digitizers:* In order to oversample the return pulse and minimize the range confusion limit, 10-b Delphi Engineering ADC3295C digitizers record both channels at two gigasamples per second (Gsps). The digitizers are triggered by the external laser timing circuit and communicate with the embedded computer over a PMC-X bus. At 25 W each, the digitizers make up the largest term of the instrument energy budget.

*6) Embedded Computer:* A major challenge in building a 2-Gsps system for the field was finding an embedded computer with sufficient bus speed. The onboard computer is a 6U Extreme Engineering Solutions XCaliber single-board compactPCI computer running Debian Linux, hosting the two digitizer cards, controlling other peripherals via USB 2.0 and making system commands, and streaming data available to an external laptop over Ethernet. The onboard DWEL control software was developed for the instrument in the Python programming language.

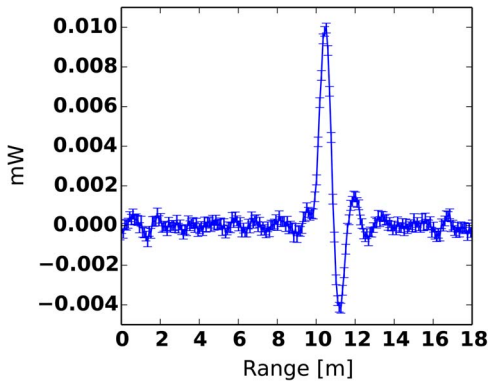


Fig. 2. Example background-subtracted waveform from a hard target at 1548 nm. Error bars are the standard deviation of the subtracted mean background.

*7) Batteries:* The instrument is powered by a pair of Ultralife UBBL09/B lithium-ion batteries, providing a combined energy of 413 W · h and weighing 2.8 kg. The pair provides over 2 h of instrument operation, allowing a day of field work for every 11.2 kg of battery mass.

*8) Motors and Encoders:* Brushless motors with ceramic planetary gear heads provide a smooth scanning motion while drawing less than 2 W each during a fast scan. Gurley Precision Instruments 12-b optical shaft encoder wheels with readout electronics provide 19 b of interpolated absolute angle resolution, greatly exceeding the design requirement.

The final assembled instrument weighs 19 kg without batteries and draws approximately 120 W while scanning.

### C. Range Dependence of Return Intensity

The DWEL instrument simultaneously records two waveform channels, time-dependent records of return intensity, which depend both on the target composition and the range. Fig. 2 shows an example waveform. Regardless of the beam profile, knowledge of the dependence of signal return strength on range is necessary to constrain the overlap function (fraction of the beam obscured) for targets of known reflectance. The receiving telescope focal length, focus, and photodetector size are fixed, such that at near ranges, the beam overfills the detector, while in the far field, the FOV and beam divergence are constant, and the return power falls off by the inverse square law. A functional form for the range dependence is derived in the following discussion.

For an ideal Lambertian target, at range $d$, much larger than the outgoing beamwidth, and diffusely reflecting an incident beam of power $P_0$ into a hemisphere, the power received at the telescope of area $A_t$ is

$$P_{Rx}(d) = P_0 A_t \frac{K(d)}{\pi d^2}. \tag{1}$$

$K(d)$ is the overlap function of the laser beam and the detector FOV or the telescope efficiency factor [1], which accounts for variations in telescope FOV with range. (Here, target albedo and calibration are set to unity for simplicity.) We will neglect atmospheric attenuation, which is small for the ranges and wavelengths of interest [14]. The first generation EVI instrument employed an efficiency factor of the form

$K(d) = 1 - \exp(-d^2/k)$ [15]. The form for the DWEL geometry must be derived, considering the Gaussian beam profile and the decreased beam size. The half-angle FOV of the DWEL telescope is defined by the ratio of the photodiode radius $R$ and the system focal length $f_{\text{sys}}$. The outgoing beam profile is an axially symmetric 2-D Gaussian function characterized by $\sigma = \sigma_0 + \theta d$, where $d$ is the distance, or range, to the target, $\theta$ is the beam divergence, and $\sigma_0$ is the initial beam radius. In polar coordinates, the normalized return power striking the detector is given by the definite integral of the 2-D Gaussian function

$$K(d) = \frac{1}{2\pi\sigma^2} \int_0^{2\pi} \int_0^{y} e^{-(r^2)/2\sigma^2} r dr d\phi \tag{2}$$

where $y$ is the FOV at the range of interest and $y = Rd/f_{\text{sys}}$. Integrating gives the correction for the dependence of the return power on range

$$K(d) = \left(1 - \exp\left[-\frac{(Rd/f_{\text{sys}})^2}{2(\sigma_0 + \theta d)^2}\right]\right). \tag{3}$$

Note that, if $\sigma_0 \gg \theta d$, then this simplifies to the EVI efficiency function, where $k = 2(\sigma_0 f_{\text{sys}}/R)^2$.

Inserting (3) into (1) and rearranging give a functional form suitable for parametric fitting to return power

$$P_{Rx}(d) = \frac{C_0}{d^2}\left(1 - \exp\left[\frac{-(C_2 d)^2}{(C_1 + d)^2}\right]\right) + C_3 \tag{4}$$

where $C_0 = (P_0 A_t/\pi)$, $C_1 = (\sigma_0/\theta)$, $C_2 = (R/\sqrt{2}\theta f_{\text{sys}})$, and $C_3$ is a background noise term.

To validate the aforementioned model of near-field behavior, return power versus range for the 1548-nm laser was measured in the laboratory from a calibrated Lambertian target. The top panel of Fig. 3 shows data and the $\chi^2$ best-fit models, calculated with the Sherpa Python module [16]; the bottom panel shows the residual difference for both models and the measured return power. The return intensity with range for the best-fit EVI efficiency (including a background term function) is shown as a thin line ($\chi^2$ probability: $P = 0.59$), and the DWEL function (4), a thick dashed line, shows a significantly improved fit ($P = 0.99$).

### D. Data Output

Rather than storing data continuously, waveform channels are recorded for a shot duration (the time of flight to the maximum range) after the lasers trigger and are saved with a processor timestamp. In the reduction process, encoder values, sampled at a lower rate, are interpolated onto shot timestamps along with a compass heading and tip-tilt sensor reading, generating a point cloud of two band brightness as a function of angle and range. Background-subtracted and range-corrected point clouds at each DWEL wavelength may be reduced following the full-waveform methods developed for EVI [1].

## IV. Early Results

A June 2013 scanning campaign in Sierra Nevada National Forest demonstrated the instrument range $> 70$ m, and Fig. 4 shows the instrument during this deployment. A histogram

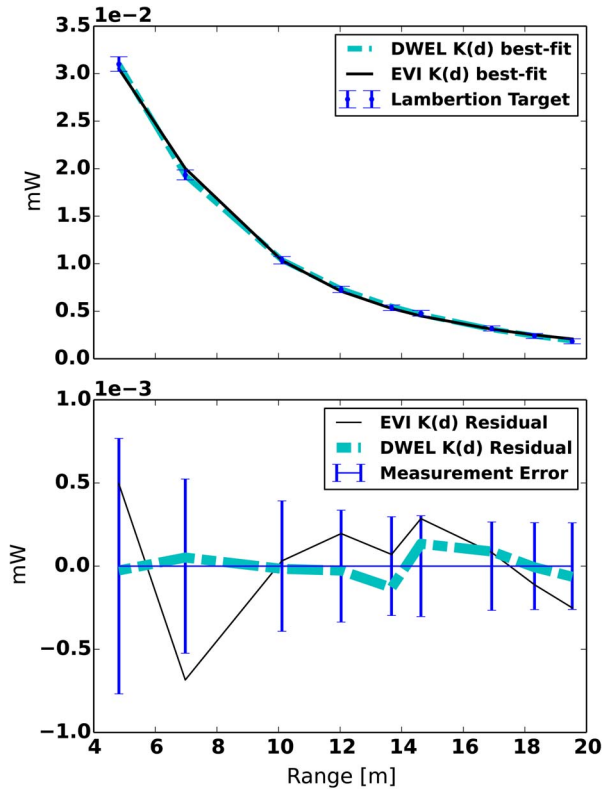


Fig. 3. Near-field range measurement test and best-fit telescope efficiency functions, using maximum return power from a Lambertian test target. The top panel shows the best-fit models, and the bottom frame shows the residuals for each model. In both panels, error bars represent the $1\sigma$ uncertainty at each range.

Fig. 4. Complete DWEL instrument deployed in the Sierra Nevada National Forest, before the case was painted bright orange.

of the normalized difference (NDI, the ratio of the intensity difference versus the intensity sum) of maximum waveform values at the two DWEL wavelengths [Fig. 5(a)] demonstrates the sharp leaf versus bark contrast. Fig. 5(b) shows a projection of the NDI in both the foreground trees and far ranges with a contrast set at the intercept of the two Gaussians.

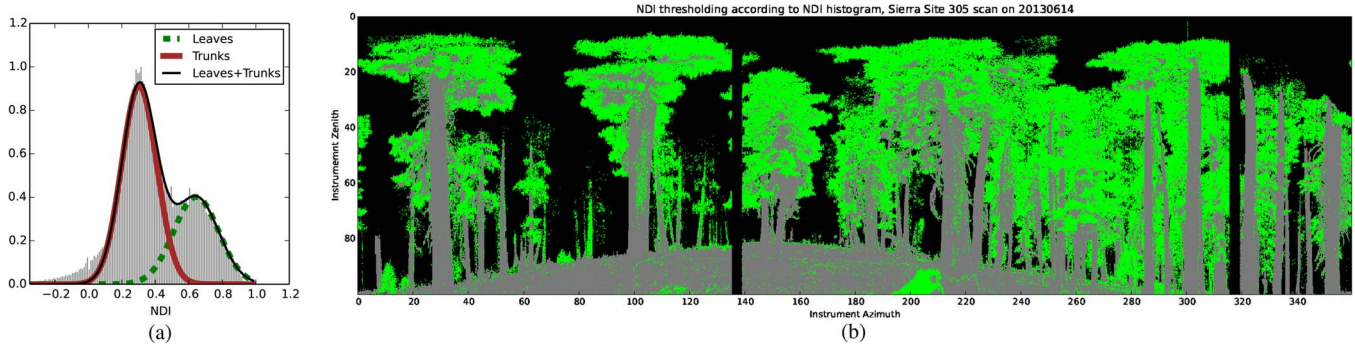


Fig. 5. Example data from a dual-wavelength scan from the Sierra Nevada National Forest, June 2013. (a) Histogram of the normalized difference of channel intensity. The bimodal distribution shows that the difference between wavelengths is smaller for trunks. The intercept between the two Gaussians, at an NDI value of 0.5, gives a first-order cutoff between leaves and trunks. To illustrate discrimination of leaves from trunks, (b) shows a projection of the NDI image with pixel color thresholded by NDI; a value below 0.5 is dark, a value above 0.5 is lightly shaded, and black indicates no return.

### A. Data Quality

In early trials, including the scan shown in Fig. 5(b), the instrument angular resolution was limited by timing errors in the encoder readout electronics. An improved readout approach has brought timing jitter down, $\sigma < 2$ mrad, for subsequent campaigns. The laser output power has been observed to drift significantly with temperature. This variation has an unavoidable impact on maximum range, which has been mitigated by increased cooling at the expense of battery life. Power changes are tracked via returns from an internal calibration target, maintaining differential calibration between the two wavelengths. DWEL's short pulse lengths and rapid sampling rate enable high-fidelity measurement and accurate quantification of the range confusion limit using a variety of extraction techniques, including pulse fitting, deconvolution, and match filtering. Such detailed calibration, as well as additional data sets and extracted forest parameters, will be the subject of forthcoming publications.

## V. Conclusion

The deployed DWEL instrument can provide a robust quantitative measure of a small-scale forest structure. The coaxial dual-wavelength operation of DWEL greatly advances the EVI full-waveform lidar by effectively discriminating between bark and leaf targets, permitting future measurement of forest biomass and leaf area, marking a significant advance in portable high-resolution full-waveform forest lidar.

## Acknowledgment

The authors would like to thank B. Hicks, C. Mendillo, and C. Hwang for their assistance in instrument integration. The Boston University Scientific Instrument Facility and Electronics Design Facility both made essential contributions to completion of the instrument. IPython was used for assorted data reduction. Echidna is a registered trademark of CSIRO.

## References

[1] D. L. B. Jupp *et al.*, "Estimating forest LAI profiles and structural parameters using a ground-based laser called Echidna," *Tree Physiol.*, vol. 29, no. 2, pp. 171–181, Feb. 2009.

[2] J. L. Lovell, D. L. B. Jupp, D. S. Culvenor, and N. C. Coops, "Using airborne and ground-based ranging lidar to measure canopy structure in Australian forests," *Can. J. Remote Sens.*, vol. 29, pp. 607–622, Oct. 2003.

[3] A. H. Strahler *et al.*, "Retrieval of forest structural parameters using a ground-based lidar instrument (Echidna)," *Can. J. Remote Sens.*, vol. 34, no. S2, pp. S426–S440, Nov. 2008.

[4] F. Zhao *et al.*, "Measuring effective leaf area index, foliage profile, and stand height in New England forest stands using a full-waveform ground-based lidar," *Remote Sens. Environ.*, vol. 115, no. 11, pp. 2954–2964, Nov. 2011.

[5] X. Yang *et al.*, "Three-dimensional forest reconstruction and structural parameter retrievals using a terrestrial full-waveform lidar instrument (Echidna)," *Remote Sens. Environ.*, vol. 135, pp. 36–51, Aug. 2013.

[6] F. Zhao *et al.*, "A comparison of foliage profiles in the Sierra National Forest obtained with a full-waveform under-canopy EVI lidar system with the foliage profiles obtained with an airborne full-waveform LVIS lidar system," *Remote Sens. Environ.*, vol. 136, pp. 330–341, Sep. 2013.

[7] T. U. Kampe, B. R. Johnson, M. Kuester, and M. Keller, "NEON: The first continental-scale ecological observatory with airborne remote sensing of vegetation canopy biochemistry and structure," *J. Appl. Remote Sens.*, vol. 4, no. 1, pp. 043510-1–043510-24, Mar. 2010.

[8] T. Fourty, F. Baret, S. Jacquemoud, G. Schmuck, and J. Verdebout, "Leaf optical properties with explicit description of its biochemical composition: Direct and inverse problems," *Remote Sens. Environ.*, vol. 56, no. 2, pp. 104–117, May 1996.

[9] G. A. Carter, "Primary and secondary effects of water content on the spectral reflectance of leaves," *Amer. J. Bot.*, vol. 78, no. 7, p. 916, Jul. 1991.

[10] R. Clark *et al.*, USGS Digital Spectral Library, splib06a, Data Series 231, 2007.

[11] E. S. Douglas *et al.*, "DWEL: A dual-wavelength Echidna lidar for ground-based forest scanning," in *Proc. IEEE IGARSS*, Jul. 2012, pp. 4998–5001.

[12] D. L. Jupp, D. S. Culvenor, J. L. Lovell, and G. J. Newnham, "Evaluation and validation of canopy laser radar (lidar) systems for native and plantation forest inventory," CSIRO Marine and Atmospheric Research Papers, Canberra, ACT, Australia, Tech. Rep. 20, 2005.

[13] E. Hecht, *Optics*, 4th ed. Reading, MA, USA: Addison-Wesley, Aug. 2001.

[14] S. D. Lord, "A new software tool for computing Earth's atmospheric transmission of near- and far-infrared radiation," NASA Tech. Memo. 103957, vol. 1, Dec. 1992.

[15] D. Jupp, private communication, 2013.

[16] B. Refsdal *et al.*, "Advanced Python scripting using Sherpa," in *Proc. ASP Conf. Astronom. Data Anal. Softw. Syst. XX.*, San Francisco, CA, USA, 2011, vol. 442, pp. 687–690.